RESEARCH ARTICLE

Computational modeling of luminal flow-driven mass transport in coronary arteries for optimizing drug-eluting stent efficacy

Ramprosad Saha[1], Somnath Choudhury[2*]

ABSTRACT

This study explores the influence of luminal flow and drug diffusivity on drug transport from a well-apposed drug-eluting stent with struts of square cross-section. A theoretical approach is adopted by constructing a numerical model that captures key aspects of the physiological environment. In this model, drug movement within the lumen is described as an unsteady convection-diffusion process, whereas transport through the arterial tissue is treated as a diffusion phenomenon. Assuming axis symmetry and employing a cylindrical coordinate system, the marker-and-cell (MAC) technique is used to solve the governing flow and transport equations for stent-mediated drug delivery. The model yields quantitative insights into how parameters such as Reynolds number and Peclet number influence wall shear stress and drug dispersion within both the lumen and the arterial tissue. The results, presented graphically, indicate that increasing the Peclet number reduces drug concentration in both regions. Furthermore, the simulations reveal two distinct recirculation zones—proximal and distal to the strut—with the distal region being notably more prominent. This finding aligns with earlier studies, thereby reinforcing the reliability of the proposed numerical model.

Keywords: Squared-shaped strut, Direction-dependent diffusion, Marker-and-Cell technique, Flow detachment zones, Shear stress along arterial walls

2010 Mathematics Subject Classification: 76D05, 76Z05, 65M06, 65Z05.

Indian Journal of Physiology and Allied Sciences (2026); DOI: 10.55184/ijpas.v78i01.546 **ISSN:** 0367-8350 (Print)

INTRODUCTION

Changes in the luminal blood flow due to arterial occlusions are frequently observed in cardiovascular diseases. Consequently, understanding the mechanisms underlying current treatments for coronary artery disease (CAD) is essential for improving therapeutic outcomes and advancing interventional techniques. Using a drug-eluting stent (DES) in the blocked artery to restore normal blood flow and administering local medication to prevent restenosis are common techniques. Despite the widespread use of DES, with millions implanted globally, there remains limited insight into the mechanisms governing the distribution and retention of drugs in arterial tissue.

Multiple treatment strategies have been utilized to manage coronary artery stenosis. Coronary artery bypass grafting (CABG) was first successfully executed by Robert H. Goetz in 1960.[1] It was long regarded as the gold standard until the introduction of percutaneous transluminal coronary angioplasty (PTCA) by Andreas Grüntzig in 1977.[2] While PTCA initially showed promise,[3] it was soon noted that a significant proportion of patients especially those with moderate stenosis experienced restenosis within six months post-procedure.[4]

A significant advancement occurred in the early 1990s with the introduction of coronary artery stents (CAS), deployed via balloon catheters. These stents reduced restenosis rates by mitigating elastic recoil and negative remodeling. The next major milestone came in 2003 with FDA approval of the first commercially available DES (Cypher stent), which, in contrast to bare-metal stents (BMS), dramatically reduced restenosis rates.[5] For a DES to be effective, it must deliver an optimal dosage of the drug at the appropriate time. The geometric properties of the stent – such as strut thickness, width, and shape – play a crucial role in determining the dynamics of drug delivery.

Recent research has addressed multiple facets of drug transport from DES, often simplifying models by neglecting luminal flow.[6–13] However, as flow-stent interactions gain prominence, it is now understood that altered flow patterns within the stented region significantly influence drug deposition and tissue distribution. Studies by Balakrishnan *et al*.[14,15] introduced coupled fluid dynamics and drug transport models in simplified geometries, revealing that the drug can accumulate not only beneath struts but also within recirculation zones formed due to flow separation. Further investigations demonstrated the effects of thrombus

[1]Department of Mathematics, Suri Vidyasagar College (under B.U.), Suri, Birbhum, West Bengal, India - 731101

[2]Department of Physics, Suri Vidyasagar College (under B.U.), Suri, Birbhum, West Bengal, India - 731101

***Corresponding author:** Somnath Choudhury, Department of Physics, Suri Vidyasagar College (under B.U.), Suri, Birbhum, West Bengal, India - 731101, Email: somnathbratati21@gmail.com

How to cite this article: Saha R, Choudhury S. Computational modeling of luminal flow-driven mass transport in coronary arteries for optimizing drug-eluting stent efficacy. *Indian J Physiol Allied Sci* 2026;78(1):18-25.

Conflict of interest: None

Submitted: 16/06/2025 **Accepted:** 11/10/2025 **Published:** 20/03/2026

characteristics and flow profiles on drug kinetics, while Kolachalama *et al*.[16,17] explored how luminal flow alters drug coverage areas and causes asymmetry in tissue drug uptake. Considering that most stent struts are trapezoidal or rounded [18], the present study focuses on luminal flow past a DES with squared struts.[19,20] The blood is treated as a Newtonian fluid, with luminal drug transport governed by an unsteady convection-diffusion equation, and tissue drug transport modeled via diffusion. The unsteady governing equations for both fluid motion and drug transport are solved numerically using the marker-and-cell (MAC) method developed by Harlow and Welch.[21] The model aims to examine the influence of factors such as Reynolds number, flow unsteadiness, Peclet number, and tissue diffusivity on wall shear stress and drug concentration in both the lumen and the tissue, using a finite-difference approach suited to complex geometries.

A lengthy axial segment of an artery, non-dimensionalized with respect to strut dimensions, serves as the model for the computational domain. Drug transport is explained by unsteady convection-diffusion equations in the lumen and diffusion equations in the tissue, whereas luminal flow is governed by unsteady Navier-Stokes and continuity equations. Appropriate boundary conditions-such as impermeability at the perivascular wall and continuity of flux at the blood-tissue interface-are applied, alongside zero drug concentration at the inlet and symmetry boundary conditions at the centerline. No-slip and Dirichlet conditions model fluid and drug behavior on various interfaces, and a steady Poiseuille profile is imposed at the inlet.

A finite-difference control-volume-based discretization on a staggered grid is employed to solve the system, with a time-stepping approach used to ensure stability. The results demonstrate that full strut-surface drug elution yields the highest arterial wall drug deposition, with luminal concentration stabilizing more rapidly than in the tissue. Notably, two distinct recirculation zones are observed proximal and distal to the strut, with the distal zone being larger. These zones expand with increasing Reynolds number. The findings of this work provide useful insights for interventional cardiologists and may inform future DES design strategies.

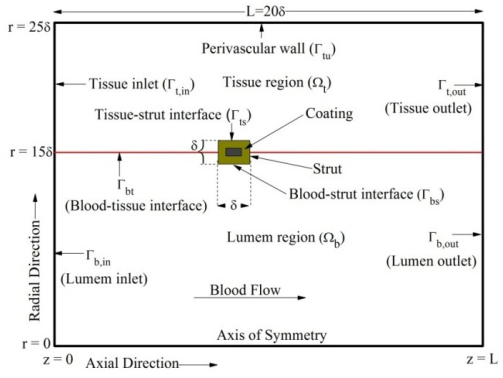

Figure 1: Schematic diagram of a stented artery

MATERIAL AND METHODS

Model Geometry

The model considers a simplified two-dimensional representation of an arterial segment (length L) aligned along the axial direction and approximated as a rectangular computational domain. The geometry is scaled by the characteristic dimension of the stent strut to obtain a dimensionless form. In this framework, the thickness of the arterial wall is assumed to be ten times the strut height, and the lumen is modeled with a width thirty times that of the strut height, following the approach described by Balakrishnan *et al*. [14] [cf. Figure 1]. The dimension-free representation of model geometry with computational grid structure is depicted in Figure 2(a).

Mathematical Formulation and Boundary Constraints

Blood flow is typically modeled as a Newtonian fluid through a stented artery. The transport of drugs in both the lumen and tissue regions is governed by convection-diffusion and diffusion equations, respectively. The dimensionless forms of the governing equations are expressed as follows:

$$\frac{\partial w}{\partial t}+\frac{\partial}{\partial r}(uv)+\frac{\partial}{\partial z}(w^2)+\frac{uw}{r}=-\frac{\partial p}{\partial z}+\frac{1}{\epsilon Re}\left[\frac{\partial^2 w}{\partial r^2}+\frac{1}{r}\frac{\partial w}{\partial r}+\epsilon^2\frac{\partial^2 w}{\partial z^2}\right], \quad (1)$$

$$\frac{\partial u}{\partial t}+\frac{\partial}{\partial r}(u^2)+\frac{\partial}{\partial z}(uw)+\frac{u^2}{r}=-\frac{1}{\epsilon}\frac{\partial p}{\partial r}+\frac{1}{\epsilon Re}\left[\frac{\partial^2 u}{\partial r^2}+\frac{1}{r}\frac{\partial u}{\partial r}-\frac{u}{r^2}+\epsilon^2\frac{\partial^2 u}{\partial z^2}\right], \quad (2)$$

$$r\frac{\partial w}{\partial z}+\frac{\partial}{\partial r}(ur)=0, \quad (3)$$

$$\frac{\partial c_f}{\partial t}+\frac{\partial}{\partial r}(uc_f)+\frac{\partial}{\partial z}(wc_f)+\frac{uc_f}{r}=-\frac{1}{\epsilon Pe_f}\left[\frac{\partial^2 c_f}{\partial r^2}+\frac{1}{r}\frac{\partial c_f}{\partial r}+\epsilon^2\frac{\partial^2 c_f}{\partial z^2}\right], \quad (4)$$

$$\frac{\partial c_t}{\partial t}=\frac{\epsilon}{Pe_t}\left[\frac{\partial^2 c_t}{\partial z^2}+\frac{1}{\epsilon^2}\frac{\partial^2 c_t}{\partial r^2}\right], \quad (5)$$

The dimensionless forms of the corresponding boundary conditions such as impermeability at the perivascular wall (Γ_{tu}) and continuity of flux at the blood-tissue interface ($\Omega_b \cap \Omega_t$) are applied,[22] alongside zero drug concentration at the lumen inlet ($\Gamma_{b,in}$) and symmetry boundary conditions at the centerline ($r=0$).[20] Zero velocity gradient at the lumen outlet ($\Gamma_{b,out}$) [14]. Drug concentration of unity at the blood-strut interface (Γ_{bs}) and tissue-strut interface (Γ_{ts}).[15] Symmetry Boundary Condition at tissue inlet ($\Gamma_{t,in}$) and tissue outlet ($\Gamma_{t,out}$).[14,23] No-slip and Dirichlet conditions model fluid and drug behavior on various interfaces ($\Gamma_{bt} \cup \Gamma_{bs}$) and a steady Poiseuille profile is imposed at the inlet ($\Gamma_{b,in}$)[23] are expressed as follows:

$$\frac{\partial c_t}{\partial r}=0 \quad on \quad \Gamma_{tu}\ , \quad (6)$$

$$D_{f/t}\frac{\partial c_f}{\partial r}=\frac{\partial c_t}{\partial r} on\ \Omega_b \cap \Omega_t, \quad (7)$$

$$\frac{\partial w}{\partial r}=0,\ u=0\ on\ r=0\ , \quad (8)$$

$$\frac{\partial c_f}{\partial r} = 0 \quad on \quad r = 0, \tag{9}$$

$$c_f = 0 \quad on\, z = 0\,, \tag{10}$$

$$\frac{\partial c_f}{\partial z} = 0 \quad on\, z = L, \tag{11}$$

$$w = 0 = u \;\; on\, r = R_b(z)\left[= \Gamma_{bt} \cup \Gamma_{bs}\right], \tag{12}$$

$$w = \left(1 - \frac{r^2}{R_b^2}\right),\; u = 0 \;\; on\, \Gamma_{b,in}, \tag{13}$$

$$\frac{\partial w}{\partial z} = 0 = \frac{\partial u}{\partial z} on\, \Gamma_{b,out}, \tag{14}$$

$$c_f = 1 \; on\, \Gamma_{bs}, \tag{15}$$

$$c_t = 1 \; on\, \Gamma_{ts}\,, \tag{16}$$

$$\frac{\partial c_t}{\partial z} = 0 \; on \; \Gamma_{t,in} \; and \, \Gamma_{t,out}, \tag{17}$$

In these equations, r and z represent the dimensionless coordinates scaled relative to the radius of the unconstricted arterial lumen (r_o), and the strut height (δ), respectively.[16,17] The z-axis lies along the symmetry axis of the artery. Here, w and u are the non-dimensional streamwise and transverse velocities of the blood, c_f and c_t are the luminal and tissue drug concentrations (normalized by the strut drug concentration), and $D_f/_t$ represents the ratio of the diffusion coefficients in the lumen and tissue. The following dimensionless numbers are defined:

$$Re = \frac{\rho U_0 r_0}{\mu}, Pe_f = \frac{r_0 U_0}{D_f}, Pe_t = \frac{r_0 U_0}{D_t}, p = \frac{\overline{p}}{\rho U_0^2}, t = \frac{\overline{t} U_0}{\delta}, \epsilon = \frac{r_0}{\delta}$$

Where U_0 is the cross-sectional average velocity at the inlet, ρ is the blood density, μ is the viscosity, D_f is the luminal drug diffusion coefficient, and D_t is the drug diffusion coefficient in the tissue 14,15.

Procedure for Obtaining the Solution

To minimize interpolation errors during the discretization of the governing equations, appropriate radial coordinate transformations are employed, defined by

$$x = \frac{r}{R_b(z)} and\; y = 1 + \frac{r - R_{tl}}{R_{tu} - R_{tl}}, where\, R_{tl} = \Gamma_{bt} \cup \Gamma_{ts}$$

These transformations map the arterial lumen onto a finite rectangular domain $[0, L] \times [0, 1]$, and the tissue region onto $[0, L] \times [1, 2]$. The finite difference method is used to numerically solve the modified governing equations, along with the associated initial and boundary conditions. Harlow and Welch's.[21] MAC (Marker and Cell) approach, which uses a control volume-based discretization on staggered grids, is used. In this grid arrangement, velocity components, pressure, and concentration values are computed at distinct locations within the control volume, as illustrated in Figure 2(b).

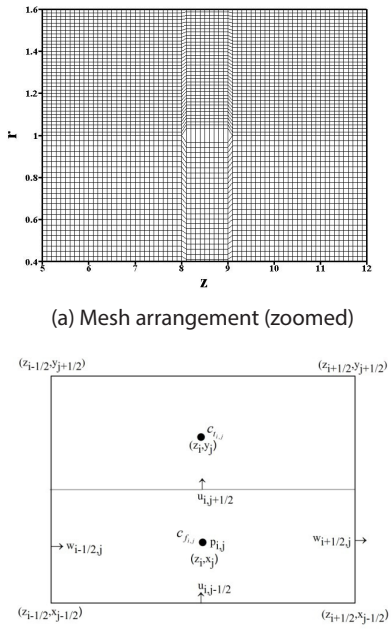

(a) Mesh arrangement (zoomed)

(b) A unified MAC cell

Figure 2: A schematic view of both the lumen and tissue

The convective terms in the momentum equations are discretized using a hybrid method that includes central differencing and second-order upwind methods, while the temporal derivatives are approximated using a first-order forward difference scheme. A second-order-accurate three-point central-difference scheme is applied to the diffusive terms.

A Poisson equation for pressure is obtained from the discretized momentum and continuity equations. This equation is iteratively solved using the successive over-relaxation (S.O.R.) technique with a relaxation parameter set to 1.2, allowing the intermediate pressure field to be computed from the velocity field. The maximum divergence of the velocity field in each cell is then evaluated and compared against a specified tolerance. If the tolerance criterion is not met, pressure values are updated throughout the domain, and the velocity field is corrected iteratively. Notably, the numerical simulations were carried out using a custom-developed FORTRAN code, without reliance on any standard computational software packages.

Stability Analysis of the Time Integration Scheme

Amsden and Harlow[24] proposed that the computational efficiency, specifically the number of calculation cycles and overall runtime, could be improved by implementing an adaptive time-stepping algorithm. This approach dynamically selects the most suitable time step based on the velocity field at each cycle. In a related study, Welch *et al.*[25] emphasized that two key stability criteria must be satisfied. The first resembles the Courant condition, which applies to a specific class of problems, whereas the second is related to the Reynolds number.

The first time-step constraint is expressed as:

$$\delta t_1 \le min\left[\frac{Re}{2}\bullet\frac{\delta z^2\delta x^2}{\delta z^2+\delta x^2}\right]_{i,j}$$

This stability criterion accounts for viscous effects [26] and can be directly employed to determine a suitable time step. A more refined approach, as adopted by Markham and Proctor.[27] among others, involves ensuring that fluid particles do not traverse more than one grid cell within a single time step. In other words,
The second time-step constraint is given by:

$$\delta t_2 \le min\left[\frac{\delta z}{|w|}\bullet\frac{\delta x}{|u|}\right]_{i,j}$$

The time-step used at any point during the calculation is determined by:

$$\delta t = a.\min\left[\delta t_1, \delta t_2\right],$$

where, $0 < a \le 1$. The inclusion of this factor helps to significantly reduce computational time, as confirmed by previous studies and our own experience.[27]

RESULTS AND DISCUSSION

The computational framework was established within a finite, non-dimensional domain, where the upstream and downstream extents were set to eight times and eleven times the non-dimensional arterial radius, respectively. Numerical solutions were obtained by generating staggered grids of size 201 × 41 for both the lumen and tissue regions. A grid independence study was conducted to evaluate the sensitivity of the results to grid resolution, the outcomes of which are depicted in Figure 3. As seen in the figure, for $Re = 500$ and $Pe_f = 5$, the velocity and concentration profiles across three different grid sizes are nearly indistinguishable, thus confirming the reliability and grid independence of the simulation results.

Figure 4 presents the axial velocity profiles at three different axial locations. All the curves indicate that the peak velocity at the arterial centerline decreases along the axis and approaches zero at both the blood-stent and blood-tissue boundaries. Notably, at the narrowest point of the square strut, there is a noticeable increase in axial velocity, which diminishes upstream and downstream from this point.

The distribution of dimensionless wall shear stress (WSS) for varying Reynolds numbers is illustrated in Figure 5, which highlights the emergence of two distinct recirculation zones on either side of the stent strut. With increasing Reynolds numbers, the length of flow separation increases, and the distal recirculation zone is noticeably greater than the proximal one. These flow-separation zones trap drug-laden blood, enhancing drug penetration into the arterial wall and promoting its accumulation at the blood-tissue interface. These results align well with earlier findings by Balakrishnan et al. [15], who analyzed drug delivery from stents with square-shaped struts.

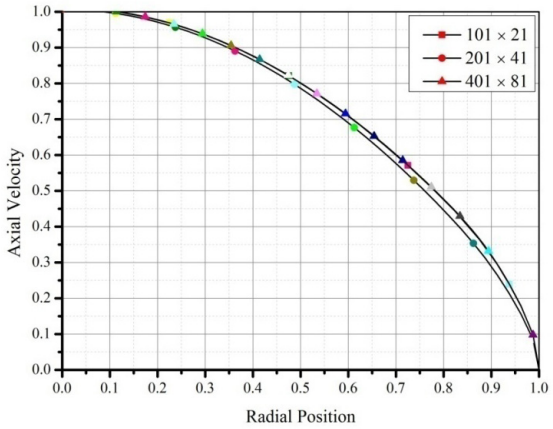

Figure 3: Axial velocity profiles for three different grid sizes

Figure 6(a-b) presents the axial variation of normalized drug concentration along a dimensionless axial coordinate in a drug-eluting stent model, comparing the effects of different Peclet numbers-which represent the ratio of advective to diffusive transport—in the lumen and tissue domains. In Figure 6(a), the lumen drug concentration is displayed *versus* axial position. The result reveals that, as Pe_f increases from 1 (black) to 10 (blue), the peak concentration decreases and shifts slightly downstream. A higher Pe_f implies stronger advection (blood flow) relative to diffusion in the lumen. This results in a more flattened and extended concentration profile, as the drug is transported more efficiently downstream before diffusing into the vessel wall. Lower Pe_f (*e.g.* $Pe_f = 1$) allows diffusion to dominate, causing the drug to accumulate more locally near the stent. Tissue drug concentration versus axial position is displayed in Figure 6(b). The result reveals that increasing Pe_t from 50 (black) to 150 (blue) causes a reduction in peak tissue concentration and a broader profile. A higher Pe_t suggests greater interstitial convection in the tissue, which transports the drug away from the site of delivery more rapidly. Thus, high Pe_t values lead to more distributed but lower concentration across the tissue depth. These plots clearly illustrate the asymmetry in drug concentration between the proximal and distal regions of the stent strut, attributable to convective transport.

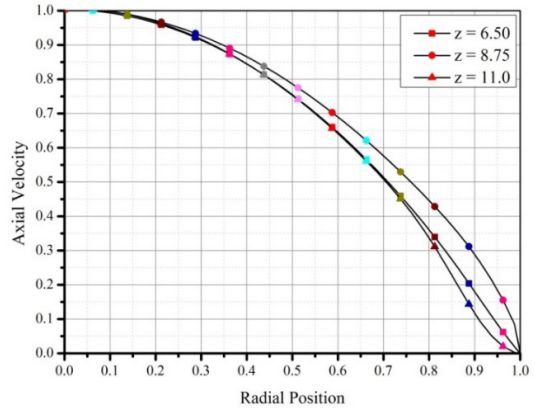

Figure 4: Axial velocity profiles for three different axial positions

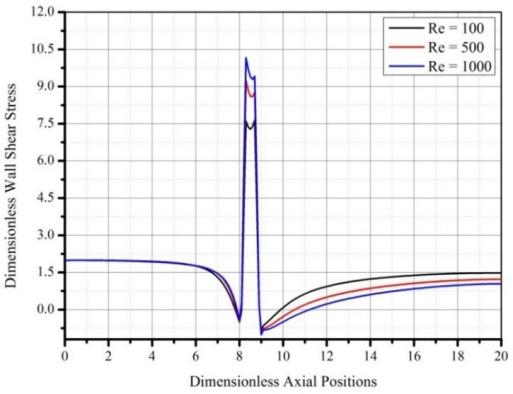

Figure 5: Axial distribution of normalized drug concentration for various Reynolds numbers

Figure 7 shows the temporal variation of normalized drug concentration in the lumen and tissue compartments for various Peclet numbers (Pe_f and Pe_t). This analyzes how drug concentrations evolve over time under the influence of convective-diffusive transport. In Figure 7 (a), the lumen drug concentration *versus* time, which indicates that the drug concentration increases rapidly at early times and reaches a quasi-steady state for all Peclet numbers. Lower Pe_f (black line, $Pe_f = 1$) results in a higher steady-state concentration in the lumen. As Pe_f increases (toward the blue line, $Pe_f = 10$), the steady-state concentration decreases. This is because higher fluid Peclet numbers indicate stronger axial advection, which flushes the drug downstream more quickly, reducing local accumulation. The tissue drug concentration versus time is depicted in Figure 7(b). It is observed that the drug concentration in the tissue shows a monotonic increase with time, gradually approaching a steady state. Lower Pe_t values (black line, $Pe_t = 50$) result in higher tissue concentrations. As Pe_t increases (toward the blue line, $Pe_t = 150$), the drug accumulation in tissue slows down and saturates at a lower value. This trend suggests that higher convective flow within the tissue hinders drug retention, as the drug is advected away before it can accumulate sufficiently.

Figure 8 provides a visual (spatial) representation of normalized drug concentration fields in both the lumen and tissue regions for varying Peclet numbers. This figure offers spatial insights that complement the axial (Figure 6) and temporal (Figure 7) concentration variations. Lumen drug concentration with different Pe_f is displayed in Figure 8(a). It is observed from the figures that, for lower $Pe_f = 1$, the drug concentration is more localized near the stent region with stronger radial penetration and accumulation. As Pe_f increases, the drug plume becomes more elongated along the axial direction, indicating dominance of convective transport. Higher Pe_f values because the drug needs to be transported further downstream, reducing radial diffusion into the tissue. The tissue drug concentration with different Pe_t is depicted in Figure 8(b). It is clear from these profiles that, at lower Pe_t, drug penetration into tissue is deeper and more symmetrical, indicating a diffusion-dominated regime. As Pe_t increases, the drug is more confined near the interface (e.g., near the lumen-tissue boundary), forming a shallower and broader front. Higher interstitial convection (high Pe_t) limits drug retention in deeper tissue, as the drug is carried away more rapidly from the site of release. These spatial contours visually reinforce conclusions that indicate the higher Peclet numbers lead to greater axial dispersion and reduced radial penetration, due to enhanced convection. Lower Peclet numbers allow greater local drug accumulation and deeper penetration into the arterial wall, favoring effective drug delivery.

Dynamic variations in drug flux across the mural interface are illustrated in Figure 9. It is observed that the instantaneous flux is closely approximated by its steady-state counterpart, implying that although drug delivery is influenced by local flow dynamics, steady-state simulations can offer valuable insights into the overall transport process.

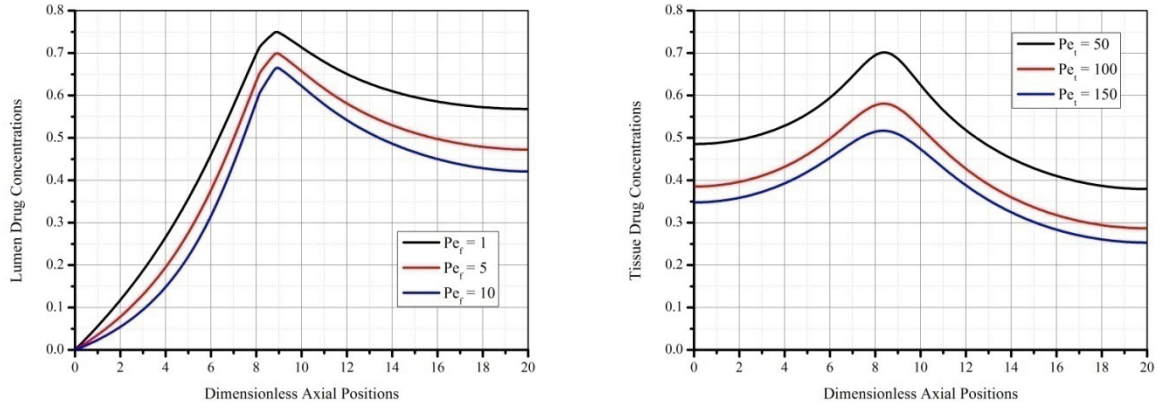

(a) Lumen drug, different Pe_f

(b) Tissue drug, different Pe_t

Figure 6: Axial distribution of normalized drug concentration for various Peclet numbers

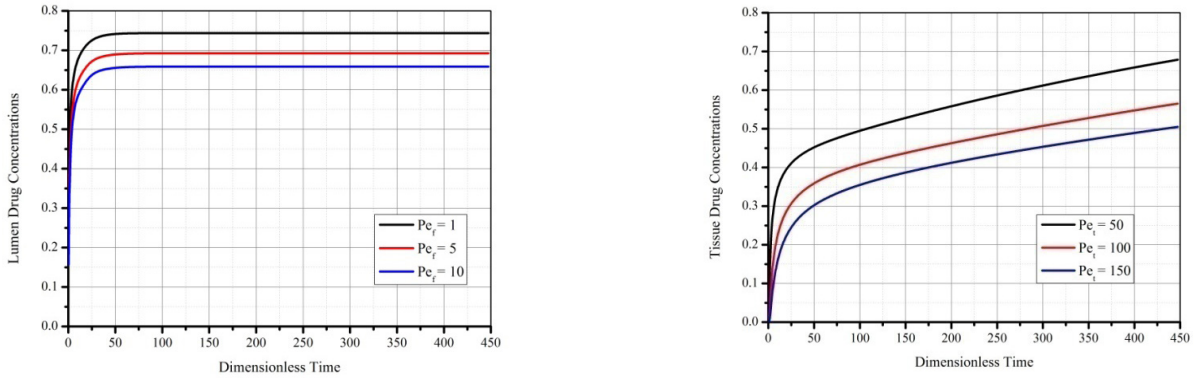

(a) Lumen drug, different Pe_f (b) Tissue drug, different Pe_t

Figure 7: Time-dependent variation of normalized drug concentration for various Peclet numbers

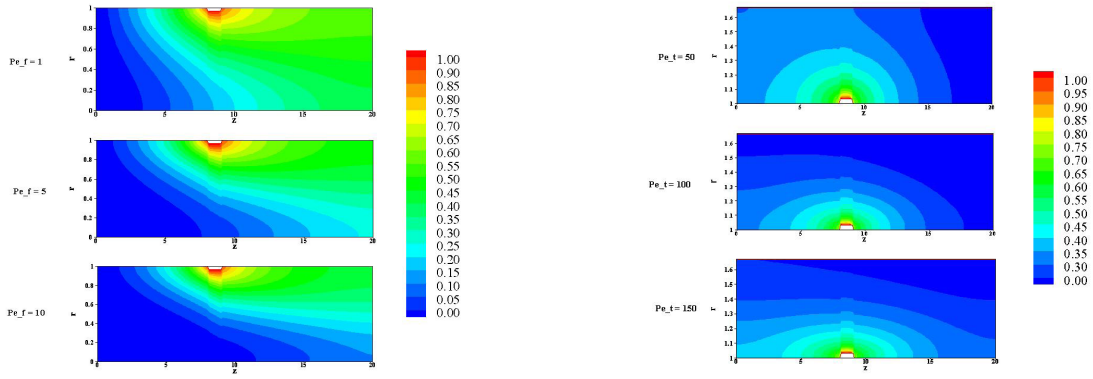

(a) Lumen drug, different Pe_f (b) Tissue drug, different Pe_t

Figure 8: Spatial distribution of normalized drug concentration under varying Peclet numbers

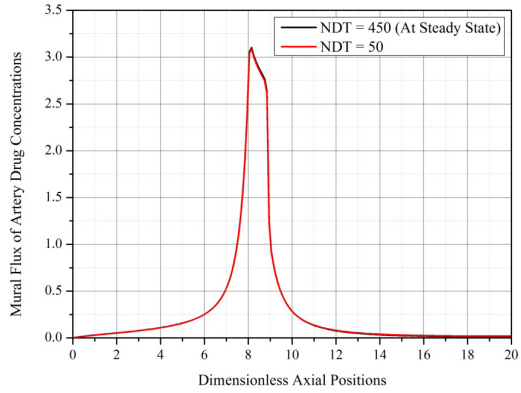

Figure 9: Normalized drug flux through the vessel wall at two distinct time points

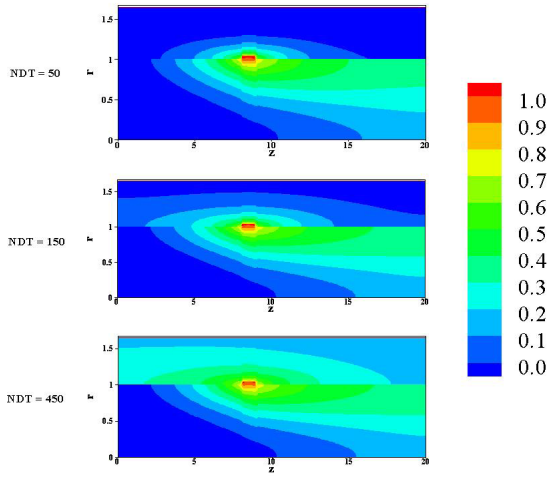

Figure 10: Spatial distribution of normalized drug concentration under varying times

Figure 10 illustrates the spatial distribution of normalized drug concentration within a domain (blood and tissue) at three non-dimensional times (NDT): 50, 150, and 450. It is clearly observed from the figure that over time, the drug transitions from being localized and intense to widespread and diluted. This temporal evolution is characteristic of diffusion-dominated transport, possibly influenced by flow (advection) if this is a blood vessel or tissue model. This observation is consistent once again with the findings reported by Balakrishnan *et al.*[14]

CONCLUSION

In this study, a two-dimensional axisymmetric model for examining drug transport and laminar blood flow from a square drug-eluting stent is presented. Drug flow in the lumen is controlled by an unsteady convection-diffusion equation, and the blood is considered to behave as a Newtonian fluid. On the other hand, an unstable diffusion model is used to simulate drug transport within the artery wall. The study reveals that tissue drug concentration reaches its peak when the drug is released from all surfaces of the stent. The computational results also indicate the presence of two separate recirculation zones—one upstream (proximal) and the other downstream (distal) of the stent strut. Interestingly, the length of flow separation rises with higher Reynolds numbers, and the distal recirculation zone is significantly greater.

As stent-based drug delivery continues to play a critical role in managing vascular diseases, several unresolved challenges regarding drug dispersion and targeting remain. For more physiologically accurate modeling in future studies, it would be beneficial to incorporate the multi-layered structure of the arterial wall and differentiate between free and bound drug interactions to better represent tissue uptake mechanisms.

ETHICAL APPROVAL

Not required.

FUNDING

No grant was received for this work.

DECLARATION OF COMPETING INTEREST

None declared.

REFERENCES

1. Goetz RH, Warren JV, Gauer OH, *et al*. Circulation of the giraffe. *Circ Res*. 1960;8(5):1049-58. DOI:10.1161/01.RES.8.5.1049.
2. Grüntzig AR, Senning Å, Siegenthaler WE. Nonoperative dilatation of coronary-artery stenosis: percutaneous transluminal coronary angioplasty. *N Engl J Med*. 1979;301(2):61-8. DOI:10.1056/NEJM197907123010201.
3. Kukreja N, Onuma Y, Daemen J, Serruys PW. The future of drug-eluting stents. *Pharmacol Res*. 2008;57(3):171-80. DOI:10.1016/j.phrs.2008.01.012.
4. Head DE, Sebranek JJ, Zahed C, Coursin DB, Prielipp RC. A tale of two stents: Perioperative management of patients with drug-eluting coronary stents. *J Clin Anesth*. 2007;19(5):386-96. DOI:10.1016/j.jclinane.2007.02.004.
5. Venkatraman S, Boey F. Release profiles in drug-eluting stents: issues and uncertainties. *J Control Release*. 2007;120(3):149-60. DOI:10.1016/j.jconrel.2007.04.022.
6. Akagawa E, Ookawa K, Ohshima N. Endovascular stent configuration affects intraluminal flow dynamics and in-vitro endothelialization. *Biorheology*. 2004;41(6):665-80. DOI:10.1177/0006355X2004041006002.
7. Duraiswamy N, Schoephoerster RT, Moreno MR, Moore Jr JE. Stented artery flow patterns and their effects on the artery wall. *Annu Rev Fluid Mech*. 2007;39:357-82. DOI:10.1146/annurev.fluid.39.050905.110300.
8. Vairo G, Cioffi M, Cottone R, Dubini G, Migliavacca F. Drug release from coronary eluting stents: a multidomain approach. *J Biomech*. 2010;43(8):1580-1589. DOI:10.1016/j.jbiomech.2010.01.033.
9. Pontrelli G, De Monte F. A multi-layer porous wall model for coronary drug-eluting stents. *Int J Heat Mass Transf*. 2010;53(19):3629-37. DOI:10.1016/j.ijheatmasstransfer.2010.03.031.
10. O'Brien CC, Finch CH, Barber TJ, Martens P, Simmons A. Analysis of drug distribution from a simulated drug-eluting stent strut using an in vitro framework. *Ann Biomed Eng*. 2012;40(12):2687-96. DOI:10.1007/s10439-012-0604-6.
11. O'Brien C, Kolachalama V, Barber T, Simmons A, Edelman E. Impact of flow pulsatility on arterial drug distribution in stent-based therapy. *J Control Release*. 2013;168(2):115-24. DOI:10.1016/j.jconrel.2013.03.014.
12. Sarifuddin, Mandal PK. Effect of Diffusivity on the Transport of Drug Eluted from Drug-Eluting Stent. *Int J Appl Comput Math*. 2016;2(2):291-301. DOI:10.1007/s40819-015-0060-8.
13. Kolandaivelu K, O'Brien CC, Shazly T, Edelman ER, Kolachalama VB. Enhancing physiologic simulations using supervised learning on coarse mesh solutions. *J R Soc Interface*. 2015;12(104):20141073. DOI:10.1098/rsif.2014.1073.
14. Balakrishnan B, Tzafriri AR, Seifert P, Groothuis A, Rogers C, Edelman ER. Strut position, blood flow, and drug deposition implications for single and overlapping Drug-Eluting Stents. *Circulation*. 2005;111(22):2958-65. DOI:10.1161/CIRCULATIONAHA.104.512475.
15. Balakrishnan B, Dooley J, Kopia G, Edelman ER. Thrombus causes fluctuations in arterial drug delivery from intravascular stents. *J Control Release*. 2008;131(3):173-80. DOI:10.1016/j.jconrel.2008.07.027.
16. Kolachalama VB, Levine EG, Edelman ER. Luminal flow amplifies stent-based drug deposition in arterial bifurcations. *PLoS One*. 2009;4(12):e8105. DOI:10.1371/journal.pone.0008105.
17. Kolachalama VB, Tzafriri AR, Arifin DY, Edelman ER. Luminal flow patterns dictate arterial drug deposition in stent-based delivery. *J Control Release*. 2009;133(1):24-30. DOI:10.1016/j.jconrel.2008.09.075.
18. Yun Z, Ai-Ke Q. Optimization of cross-section of stent wire in trapezoidal shape for the treatment of intracranial aneurysm. In: *World Congress on Medical Physics and Biomedical Engineering May 26-31, 2012, Beijing, China.* ; 2013:1338-41. DOI:10.1007/978-3-642-29305-4_351.
19. Mongrain R, Faik I, Leask RL, Rod'C J, Bertrand OF. Effects of diffusion coefficients and struts apposition using numerical simulations for drug eluting coronary stents. *J Biomech Eng*. 2007;129(5):733-42. DOI:10.1115/1.2768381.
20. Zhu X, Pack DW, Braatz RD. Modelling intravascular delivery from drug-eluting stents with biodurable coating: investigation of anisotropic vascular drug diffusivity and arterial drug distribution. *Comput Methods Biomech Biomed Engin*. 2014;17(3):187-98. DOI:10.1080/10255842.2012.672815.
21. Harlow FH, Welch JE, others. Numerical calculation of time-dependent viscous incompressible flow of fluid with free surface. *Phys Fluids*. 1965;8(12):2182. DOI:10.1063/1.1761178.
22. Khakpour M, Vafai K. Critical assessment of arterial transport models. *Int J Heat Mass Transf*. 2008;51(3):807-22. DOI:10.1016/j.ijheatmasstransfer.2007.04.021.
23. O'Connell BM, Walsh MT. *Arterial Mass Transport Behaviour of Drugs from Drug Eluting Stents*. INTECH Open Access Publisher;

2012. DOI:10.5772/19924.
24. Amsden AA, Harlow FH. *The SMAC Method: A Numerical Technique for Calculating Incompressible Fluid Flows*.; 1970. Available at https://catalog.hathitrust.org/Record/101827789.
25. Welch JE, Harlow FH, Shannon JP, Daly BJ. *The MAC Method*. Los Alamos Scientific Laboratory of the University of California; 1966.DOI:10.2172/4563173.
26. Hirt CW. Heuristic stability theory for finite-difference equations. *J Comput Phys*. 1968;2(4):339-55.DOI: 10.1016/0021-9991(68)90041-7.
27. Markham G, Proctor M V. Modifications to the two-dimensional incompressible fluid flow code ZUNI to provide enhanced performance. *CEGB Rept TPRD/L/0063/M82*. Published online 1983. DOI: 10.2172/4563173.

PEER-REVIEWED CERTIFICATION

During the review of this manuscript, a double-blind peer-review policy has been followed. The author(s) of this manuscript received review comments from a minimum of two peer-reviewers. Author(s) submitted revised manuscript as per the comments of the assigned reviewers. On the basis of revision(s) done by the author(s) and compliance to the Reviewers' comments on the manuscript, Editor(s) has approved the revised manuscript for final publication.